Ordering of Atomic Monolayers on a (001) Cubic Crystal Surface

Laurent Proville*

Groupe de Physique des Solides, UMR 7588-CNRS, Universités Paris 7 & Paris 6, 2 place Jussieu 75251, Paris Cedex 05, France

(Received 31 August 2001; published 8 January 2002)

The self-organization of a chemisorbed monolayer is studied as a two-dimensional ordering process in the presence of surface stress. As proved previously for a single phase separation, a steady surface state is yielded from the competition between the domain boundary energy and the surface stress elastic energy. In the present Letter, the resulting patterns are shown to depend on the interplay between the symmetries of both the internal layer order and the underlying crystal. For experimental relevance, our study is focused on a (001) copper surface.

DOI: 10.1103/PhysRevLett.88.046102 PACS numbers: 68.43.Hn, 64.70.Nd, 68.43.Jk, 81.40.Jj

The growth of a nanostructure onto solid surfaces provides us with promising technical perspectives for the electronic miniaturization as for the heterogeneous catalyzer assembling. The monolayer self-organization (SO) on a crystal surface is an efficient way to control the nanostructure growth by constructing a template with regular nanometer sizes and spacings. The matter which may be deposed subsequently on this template is likely to organize with the same patterns as the monolayer.

Recent analysis of chemisorbed monolayers on (001) copper surfaces, via scanning tunneling microscopy (STM) [1–3] and spot profile analyzing low-energy electron diffraction [4] showed both a large panel of morphologies and the means to control their formations.

The interplay between the long range elastic interaction yielded by the underlying crystal surface stress and the domain boundary energy has been well known to control the surface SO since the papers of Marchenko [5] and Vanderbilt *et al.* [6,7]. While Refs. [5,6] address the cases of the vicinal surfaces and the surface reconstruction, Ref. [7] was performed in the very general context of a two-phase system with $1/r^3$ isotropic dipolar interactions in two dimensions, and thus the latest study is now used to get an insight into the chemisorbed monolayer SO. Indeed, considering an assembly of surface domains inside which are fixed adatoms, the energy cost F_{chem} due to the boundary, i.e., where the adatom environment is unfavorable, is proportional to the total boundary length L, i.e., $F_{\mathrm{chem}} = I \times L$. The constant I is the boundary energy per unit length. As for a given coverage, the total domain perimeter L is minimum for a single compact domain; the smaller the number of compact domains, the weaker the domain boundary energy. On the other hand, if a non-negligible crystal surface stress Λ is associated with the adatom adsorption, the surface stress inhomogeneities induce some forces that are located at the domain boundaries. These forces yield a crystal strain, and thus an elastic work is involved which is minimum when the forces are separated by a distance as large as possible. So the surface ground state structure should balance the interplay between the boundary energy and the elastic work, and the calculations of [5–7] neatly proved that periodic domains occur with a period selection which increases exponentially with the ratio I/Λ^2, with a suitable multiplier which depends on the material elastic constants.

In Ref. [8], the 2D Cahn-Hilliard (CH) theory was proved to be an efficient tool for studying the SO kinetics on a (001) cubic crystal surface provided the elastic anisotropy due to the underlying crystal symmetries is taken into account in the calculation of the total free energy F. The 2D CH equation was assumed to drive the surface diffusion of the adatoms; i.e., the time evolution of the local adatom coverage θ is given by

$$\frac{\partial\theta(\mathbf{r},t)}{\partial t} = M_\theta \,\triangle\, \frac{\delta F}{\delta\theta(\mathbf{r},t)}\,. \tag{1}$$

A complete analysis of this equation can be found in Refs. [9,10] with no elastic interactions. The 2D CH model was also proposed for phase separation in the binary epilayer in Refs. [11] and for spinodal decomposition of a crystal surface in Ref. [8,12].

The approach developed in Ref. [8] was actually devoted to a single phase separation on a crystal surface, no matter how the internal layer order may play a role. In what follows, we describe how to take into account the symmetries of both the adatom monolayer and the underlying cubic crystal. These features are proved to determine the patterning of the steady monolayer state. Comparison with experiments is also proposed as an example of how to interpret our results.

Some additional order parameters (OP), denoted η_j with $j = 1, 2, \ldots, N$, are required to describe ordered phases that may coexist with either orientational or translational variants. The number N of distinct OP's depends on the number of variants as described below for some examples. The kinetics is thus completed by a set of N Allen-Cahn equations:

$$\frac{\partial\eta_j(\mathbf{r},t)}{\partial t} = -M_\eta\,\frac{\delta F}{\delta\eta_j(\mathbf{r},t)} \tag{2}$$

that control the time evolution of each nonconserved parameter η_j. Such an approach was developed in metallurgical science by Khachaturyan [13] for the microstructure

ordering in alloys. As we found no experimental results about the ordering kinetics of the surface, M_η is an adjustable parameter which is assumed to fulfill the adiabatic regime; i.e., the ordering kinetics is much faster than the matter diffusion. The mobility constant M_θ is proportional to the Fick diffusion coefficient which is around 10^{-6} cm^2/s at 300 K (see [14]).

The total surface free energy F can be written as a sum of two terms, i.e., first a chemical term F_{chem} which includes both the energy due to covalent bonds substrate adatoms and the subsequent entropy, and second a long range elastic term E_{el} due to the crystal surface stress which is imposed by the presence of adatoms. In the framework of a continuous approach, both F_{chem} and E_{el} may be expanded with respect to the coverage θ, the η_j's, and their respective surface gradients. Let us first write F_{chem} as a Ginzburg-Landau functional:

$$F_{\text{chem}} = F_0 \iint_S \left\{ \frac{\gamma_\theta}{2} [\nabla_s \theta]^2 + \frac{\gamma_\eta}{2} \sum_j [\nabla_s \eta_j]^2 + \hat{f}(\theta) \right\} d\mathbf{r} . \quad (3)$$

We introduce here the adimensional free energy density,

$$\hat{f} = A\theta^2 + E_2(\theta_1 - \theta) \sum_i \eta_i^2 - E_3 \eta_1 \eta_2 - E_4 \sum_i \eta_i^4 + E_5(\eta_1 \eta_2)^2 + E_6 \sum_i \eta_i^6, \quad (4)$$

and the surface gradient $\nabla_s = [(\partial/\partial x_1)^2 + (\partial/\partial x_2)^2]$, where (x_1, x_2) are the surface coordinates along the (100) and (010) directions of the (001) cubic crystal surface. The F_0 and γ_η, γ_θ scalars are, respectively, the free energy density constant and the amplitudes of the gradient term that both are adjusted to set the model domain boundary energy I to a realistic value, i.e., around 10 meV/Å (see Refs. [6,15]).

As the OP are supposed to describe the different variants of the internal layer structure, it is required that any symmetry operation relative to this structure should change the η_j's leaving unchanged the $\hat{f}$ quantity. For simplicity, the polynomial $\hat{f}$ expansion is truncated after the sixth OP power, and we focus on a case with only two OP's which is sufficient to study basic structures such as C2X2 and P2X1, well known from surface scientists [see Fig. 1 for the case of a (001) fcc surface].

The C2X2 has two variants passing from one to the other by a [1 1 0] surface vector translation. In our formalism, this structure can be represented by two $\hat{f}$ minima for $\theta = 1$ and with either $\eta_1 = \eta_2 = 1$ or $\eta_1 = \eta_2 = -1$ depending on which variant is considered. The internal order P2X1 correspond to two orientational variants since the adatoms may arrange either along the direction [110] or $[1\bar{1}0]$, and for each orientation there are two translational variants, passing from one to the other by a translation of [2 0 0]. This structure may correspond to four $\hat{f}$ minima at $\theta = 1$ and with either $\eta_1 = \pm 1$ and $\eta_2 = 0$ or $\eta_2 = \pm 1$ and $\eta_1 = 0$. As a result of the P2X1 symmetries, the coupling coefficient E_3 in Eq. (4) must be zero. Minimizing the $\hat{f}$ potential with respect to OP's for a given θ value gives two kind of minima, i.e., one disordered surface for which the whole set of OP is zero and some ordered surfaces for which the OP's have nonzero values. The $\hat{f}$ coefficients are adjusted such as plotting the $\hat{f}$ potential after minimizing with respect to the OP's gives a double-well potential with two minima at $\theta = 0$ and $\theta = 1$.

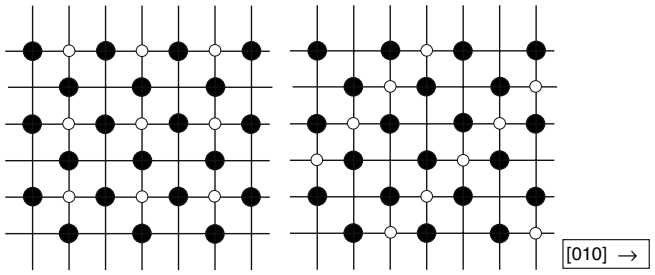

FIG. 1. On a (001) fcc crystal surface (atoms of which are represented by full circles), the adatoms (empty circles) may arrange in a perfect C2X2 order (on the left-hand side) or in a P2X1 order (on the right-hand side). The direction [010] is indicated.

The E_{el} energy is calculated by inverting the mechanical equilibrium equations, assuming a surface external force distribution $\mathbf{P}$ which is due to the adsorption. At the surface, we have

$$\sigma_{i,j}(\mathbf{r}, x_3 = 0) \cdot n_j = P_i(\mathbf{r}) , \quad (5)$$

where n_j is a component of the surface normal $\mathbf{n} = [001]$ and the summation over subscript j is implicit. The crystal bulk stress, $\sigma_{i,j}(\mathbf{r}, x_3)$ is due to the crystal displacements $\mathbf{u}(\mathbf{r}, x_3)$ and it is given by the Hooke law: $\sigma_{i,j} = \lambda_{i,j,k,l} \partial u_k / \partial x_l$. The forth order tensor $\lambda_{i,j,k,l}$ gives the crystal elastic constants and, for a cubic crystal symmetry, this tensor is composed with three nonzero coefficients [16], namely, $\lambda_{i,i,i,i} = C_{11}$, $\lambda_{i,i,j,j} = C_{12}$, and $\lambda_{i,j,i,j} = \lambda_{i,j,j,i} = C_{44}$. The bulk displacements fulfill the Lamé equation:

$$\lambda_{i,j,k,l} \frac{\partial^2 u_k}{\partial x_j \partial x_l} = 0 . \quad (6)$$

Equations (5) and (6) are inverted by writing the displacements as two-dimensional Fourier transforms of which the Fourier components depend on both a surface wave vector $\mathbf{Q} = (q_1, q_2)$ and the deepness x_3 inside the bulk. As detailed in [8], it gives the surface elastic Green function $G_{i,l}(\mathbf{Q})$. The crystal elastic energy is given by an analytical expression in the Fourier space:

$$E_{\text{cry}} = -1/2 \int_{x_3=0} \tilde{P}_i^* [G_{i,l}] \tilde{P}_l \, d\mathbf{Q} , \quad (7)$$

where $\tilde{P}_j$ is the P_j Fourier transform.

We now detail how the external force $\mathbf{P}$ is derived. Let us denote σ^0 to be the surface stress imposed to the crystal by the chemisorbed monolayer, i.e., $\sigma^0 = 0$ on the free surface and $\sigma^0 \neq 0$ in the adsorbate domains. Assuming

that the monolayer is a perfect plan, the stress σ^0 is given by a 2×2 tensor, and the induced force $\mathbf{P}$ is simply obtained by deriving σ^0 with respect to the surface coordinates, which gives

$$P_i = \sum_{l=1,2} \frac{\partial \sigma^0_{il}}{\partial x_l}. \quad (8)$$

The stress tensor σ^0 can be expanded with respect to the local coverage θ and the OP's, i.e., η_1 and η_2. On one hand, if no anisotropy appears in the layer structure, which is the case for a disordered layer or when there is no orientational variants, e.g., the C2X2, then we write $\sigma^0(\mathbf{r}) = \sigma^{00}\theta(\mathbf{r})$, where we introduce the constant tensor σ^{00} which verifies $\sigma^{00}_{12} = \sigma^{00}_{12} = 0$ and $\sigma^{00}_{11} = \sigma^{00}_{22} = \Lambda$. On the other hand, if there are orientational variants, one must add a correction to $\sigma^{00}\theta(\mathbf{r})$ and we propose to write

$$\sigma^0(\mathbf{r}) = \sigma^{00}\theta(\mathbf{r}) + \sum_{j=1,2} \sigma^{0j}\eta_j(\mathbf{r})^2. \quad (9)$$

This expansion holds when the OP's correspond one-to-one to the structure orientations, which is the case for the P2X1 order. We focus on the P2X1 orientational variant where first adatom neighbors are placed along the [110] direction (Fig. 1). Let us denote Λ_1 and $\Lambda_{\bar{1}}$ to be the amplitudes of the stress along [110] and $[1\bar{1}0]$, respectively. We have $|\Lambda_1| > |\Lambda_{\bar{1}}|$ because of the proximity of first adatom neighbors which reveals the internal structure anisotropy. After performing a suitable rotation, the stress tensor is written in the repair $[100] \times [010]$ as follows: $\sigma^0_{11} = \sigma^0_{22} = \Lambda$ and $\sigma^0_{12} = \sigma^0_{21} = \mu$, where $\Lambda = 0.5(\Lambda_1 + \Lambda_{\bar{1}})$ and $\mu = 0.5(\Lambda_1 - \Lambda_{\bar{1}})$. We now identify Eq. (9) for a perfect P2X1 ordered domain with the suitable orientational variant which gives the same expression σ^{00} as for the C2X2 phase but with nonzero off-diagonal coefficients for the σ^{01} tensor: $\sigma^{01}_{12} = \sigma^{01}_{21} = \mu$. The same can be done with the other P2X1 orientational variant and it gives $\sigma^{02}_{12} = \sigma^{02}_{21} = -\mu$. As Λ_1 and $\Lambda_{\bar{1}}$ are assumed to have the same sign which means that a dilation (or compression) occurs in both directions [110] and $[1\bar{1}0]$, it implies $|\mu| < |\Lambda|$.

For the chemisorbed compounds such as atomic nitrogen or oxygen, a 2D film with atomic thickness would not be stable without first being adsorbed on a suitable substrate. Therefore, there is no equilibrium state with respect to which the monolayer strain field can be measured. Consequently, the relevant parameter to develop the elastic energy of the monolayer E_{lay} is the stress σ^0 and, as E_{lay} is degenerate with respect to the sign of the stress, we have

$$E_{\text{lay}} = \iint_S \beta_{ijkl}\sigma^0_{ij} \cdot \sigma^0_{kl}\, d\rho\,, \quad (10)$$

where the constant tensor β is introduced to fix the intrinsic elastic properties of the atomic layer. The total elastic energy of the surface is thus $E_{\text{el}} = E_{\text{cry}} + E_{\text{lay}}$, but the exact computation of E_{lay} is rather difficult as we have no estimation of β. Nevertheless, one notes that E_{lay} is simply a sum of the surface integral of the functions θ^2, η_j^4, and $\theta\eta_j^2$, so its contribution to the total free energy is equivalent to a rescaling of the adimensional coefficients of the free energy density $\hat{f}$. From the experimental point of view, the layer elastic energy can neither be measured separately nor be neglected when measuring the growth rate of an alone domain (at very low coverage) which provides an evaluation of the boundary energy I. Therefore adjusting the model boundary energy I to a realistic value as we did yet includes the contribution of E_{lay}.

Let us restate the model parameters: $I = 10$ meV/Å, $\Lambda = 40$ mJ/m^2 ($\Lambda = 0.25$ eV/Å^2), and the elastic constants of copper $C_{11} = 1.683$, $C_{12} = 1.221$, $C_{44} = 0.757$ which unit is 10^{11} J/m^3 [17]. Equations (1) and (2) are integrated with a finite space and time element method. The kinetics starts from a uniform coverage $\theta = \theta_0$ and a uniform random distribution of OP's between -1 and 1. The adimensional coefficients of the $\hat{f}$ polynomial expansion are for the C2X2 structure $A = 31$, $E_2 = 124$, $E_3 = 29$, $E_4 = 0$, $E_5 = E_6 = 155$, $c_1 = 0.31$, and for the P2X1 structure $A = 10$, $E_2 = 40$, $E_3 = 0$, $E_4 = 21.3$, $E_5 = 57$, $E_6 = 50$, $c_1 = 0.35$.

On a (001) cubic crystal surface, the ordering process is shown to lead to a steady state with different mesoscopic patterns according to the coverage and the internal structure (see Fig. 2). Because of the crystal cubic symmetry and the monolayer internal structure, the final state differs from the one predicted in Refs. [5–7]. Nevertheless, the space correlation function of the final state, i.e., $\langle\theta(\mathbf{r} + \boldsymbol{\tau})\theta(\mathbf{r})\rangle$ exhibits a characteristic wavelength which decreases exponentially with the boundary energy per unit length I which confirms the predictions established in [5,6].

For a perfect C2X2 internal structure, no internal anisotropy is induced. Only the symmetries of the underlying crystal play a role in the patterning. At low

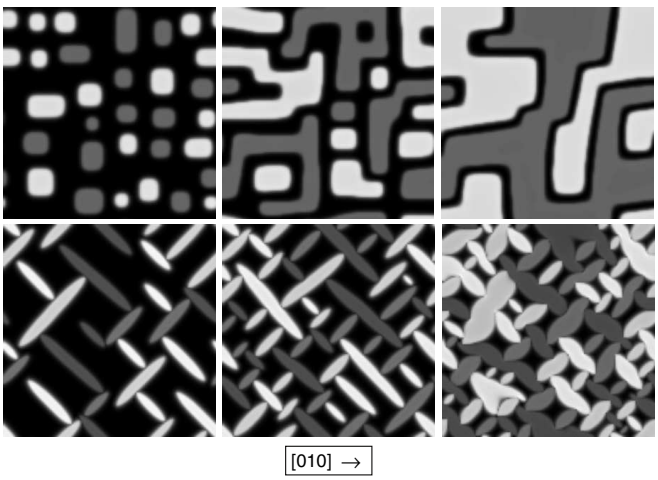

FIG. 2. Phase separated final state on a (001) copper crystal surface with $\Lambda = 40$ mJ/m^2 (defined in the text) for a C2X2 (first row) at $\theta_0 = 0.25$ (on the left), $\theta_0 = 0.5$ (in the middle), $\theta_0 = 0.75$ (on the right-hand side), and for a P2X1 (second row) with $\mu = 0.9\Lambda$ at $\theta_0 = 0.38$ (on the left), $\theta_0 = 0.5$ (in the middle), and $\theta_0 = 0.75$ (on the right-hand side). The gray scale enhances the different variants of the layer structures. The direction [010] is indicated.

coverage $\theta_0 = 0.25$, the phase separation kinetics yields a nanostructure of square-shaped islands arranged in raft along either the [100] or the [010] directions that are the elastic soft directions of the copper surface. The two translational variants are identified with two different shades of gray. Increasing coverage θ_0, the surface shows a crossover going from square-shaped droplet structures at low coverage to a labyrinthine structure for $\theta_0 > 0.5$, passing through mixed structures. The labyrinthine structure occurs with two kinds of walls according to the translational variants of the ordered phase. For θ_0 values in the crossover range, the branched stripes coexist with droplets (see Fig. 2 for $\theta_0 = 0.5$). When coverage becomes large enough $\theta_0 > 0.65$, the monolayer undergoes another shape transformation which yields large compact domains. For $\theta_0 = 0.75$, the situation is not the counterpart of a surface with $\theta_0 = 0.25$ (see Fig. 2) as one would expect from a simple phase separation. Some antiphase boundaries (APB) due to the coexistence of different order appear as trenches between the neighboring domains. The present theoretical results about a (001) copper surface with a C2X2 monolayer may be compared with what is experimentally observed in [1,2] with the STM analysis of the N/Cu(001) system. The atomic precision of the STM enhanced adatom missing rows which our model cannot capture because of the coarse graining. In the experiments, those missing rows occur every 5.2 nm along both [100] and [010] directions and thus the adatom layer appears as an assembly of square-shaped islands with 5.2 nm size. According to Leibsle *et al.* [1], those missing rows are due to the lattice parameter mismatch between the bulk lattice constants of Cu_3N and the (001) copper surface unit cell. Nevertheless, if one considers the islands separated by missing rows as a single domain, then the final state patterns enhanced by the STM experiments are very similar to the ones shown in the first row of Fig. 2, for different coverage. Indeed, the C2X2 structure with missing rows might be consider as a nonperfect C2X2 with no internal anisotropy as the perfect C2X2.

The P2X1 order implies a layer internal anisotropy, i.e., $\mu \neq 0$. In the second row of Fig. 2, it is shown that the patterns strongly differ from the C2X2 case. The domains appear as tips, sides of which are oriented along specific directions. The weaker is $(1 - \mu/\Lambda)$, i.e., the stronger is the internal anisotropy, the thinner are the tips, and their sides tend to align with either [110] or $[1\bar{1}0]$. The second row of Fig. 2shows the different patterns according to the coverage for $\mu = 0.9\Lambda$ which is close to the μ upper limit. The tips with different variants do not branch to each other because of the APB, and the growth of some domains may be stopped by their neighbors with different orientations.

The anisotropy factor of a cubic crystal is given by the combination of the elastic constants $\chi = C_{11} - C_{12} - 2C_{44}$ (see Ref. [16]). For example, copper and gold χ's are negative ($\chi_{Cu} = -1.0, \chi_{Au} = -0.5$), and chromium and niobium χ's are positive ($\chi_{Cr} = +1.8, \chi_{Nb} = +0.5$). The case $\chi < 0$ as for copper is described above while, for a positive χ, the soft elastic directions of the crystal surface are [110] and $[1\bar{1}0]$ instead of [100] and [010] for a negative χ. For $\chi > 0$, our calculations showed that the internal anisotropy of a P2X1 layer does not modify the preferential orientations of domains due to the crystal symmetries. Only the shape of the domains is changed at low coverage passing from square islands arranged in raft along [110] and $[1\bar{1}0]$ when $\mu = 0$ to long tips aligned in the same directions when $\mu > 0$. A C2X2 layer deposited on a cubic crystal with $\chi > 0$ gives the same patterns as a P2X1 layer with $\mu = 0$: The domain sides are aligned with either [110] or $[1\bar{1}0]$ instead of [100] or [010].

In summary, it is proved that the patterning which is yielded by the ordering of the atomic monolayer onto the crystal surface is controlled by the symmetries of both the internal layer structure and the underlying crystal. Our results about the ordering of a C2X2 layer on a copper surface are in good agreement with the experiments. The method we used in the present paper is a promising tool to study the surface nanostructures.

*Present address: Laboratoire de Minéralogie Cristallographie Paris, UMR 7590-CNRS, Universités Paris 6 & Paris 7, 4 pl. Jussieu 75252, Paris Cedex 05, France.
Web address: http://www.lmcp.jussieu.fr/

[1] F. M. Leibsle *et al.,* Phys. Rev. B **47**, 15 865 (1993).
[2] H. Ellmer *et al.,* Surf. Sci. **476**, 95 (2001).
[3] T. W. Fishlock *et al.,* Surf. Sci. **445**, 47 (2000).
[4] M. Sotto and B. Croset, Surf. Sci. **461**, 78 (2000).
[5] V. I. Marchenko, Sov. Phys. JETP **54**, 605 (1981).
[6] O. L. Alerhand *et al.,* Phys. Rev. Lett. **61**, 1973 (1988).
[7] Kwok-On Ng and David Vanderbilt, Phys. Rev. B **52**, 2177 (1995).
[8] L. Proville, Phys. Rev. B **64**, 165406 (2001).
[9] J. D. Gunton *et al., Phase Transitions and Critical Phenomena,* edited by C. Domb and J. L. Lebowitz (Academic, New York, 1983), Vol. 8, p. 269.
[10] A. J. Bray, Adv. Phys. **43**, 357 (1994).
[11] Z. Suo and L. Lu, J. Mech. Phys. Solids **42**, 211 (2000); **49**, 1937 (2001).
[12] J. Stewart and N. Goldenfeld, Phys. Rev. A **46**, 6505 (1992).
[13] A. G. Khachaturyan, *Theory of Structural Transformations in Solids* (Wiley-Interscience, New York, 1983), Chap. 7; Yunzhi Wang, L. Q. Chen, and A. G. Khachaturyan, in *Computer Simulation in Materials Science: Nano/Meso/Macroscopic Space and Time Scales,* edited by H. O. Kirchner, L. P. Kubin, and V. Pontikis, NATO ASI, Ser. E Vol. 308 (Kluwer Academic, Boston, 1996), pp. 325–371.
[14] A. Zangwill, *Physics at Surfaces* (Cambridge University Press, Cambridge, England, 1988), p. 380.
[15] B. Croset *et al.* (to be published).
[16] E. M. Lifshitz and L. D. Landau, *Theory of Elasticity*, Theoretical Physics Vol. 7 (Butterworth-Heinemann, Stoneham, MA, 1995), 3rd ed., pp. 54–55.
[17] See any standard physics handbook.